A Physics-Inspired Design Paradigm for Novel Dynamics in Non-Holomorphic Maps (Revised)

Vincent Marquez
Independent Researcher
vincentmarquez40@yahoo.com
GitHub: https://github.com/VincentMarquez
ORCID: 0009-0003-5385-056X

July 17, 2025

Abstract

This study introduces and validates a design paradigm for discovering complex dynamical systems by repurposing mathematical operators from physical models. We begin with a foundational analysis of a driven nonlinear optical cavity, then deconstruct its governing equation into functional components to engineer a novel class of discrete-time maps. The resulting systems are non-holomorphic, a property essential for their unique dynamics. We term the emergent behavior "frustrated bounded chaos": the generation of bounded chaotic attractors arising from a balance between nonlinear expansion and a countervailing, magnitude-dependent recoil. Computational diagnostics confirm genuine chaos with a positive Lyapunov exponent $\lambda_1 = 0.155 \pm 0.030$, placing the system in the weak chaos regime while maintaining confinement. A computational search of 10,000 map variations, seeded by 10 distinct, physics-inspired equations, was conducted to validate the paradigm. The results demonstrate that this principled design approach enables tunable chaos—the ability to switch between chaotic and contractive regimes through single-parameter adjustments. We conclude by discussing the properties of this dynamical class, proposing a schematic for physical realization, and analyzing how the frustrated mechanism creates the coexistence of exponential sensitivity and spatial confinement.

1 Introduction

The inverse design of systems with specific, complex behaviors is a central challenge in fields ranging from photonics to materials science. While physical models excel at predicting the behavior of a given system, a systematic methodology for creating novel systems with desired properties like stability and structural richness remains an open area of research. Nonlinear optical cavities, which manifest phenomena like optical bistability and lasing through a delicate balance of driving, dissipation, and nonlinearity, offer a particularly fertile ground for exploring these principles, from the generation of dissipative solitons to complex pattern formation [1, 2, 8, 9]. Understanding and harnessing these dynamics is crucial for advancing photonic technologies, from all-optical switches to the generation of exotic states of light [7].

This investigation adopts a dual strategy that reflects the interplay between physical intuition and mathematical innovation. First, we perform a rigorous analysis of a standard model for a driven, dissipative nonlinear optical cavity to establish a physical baseline (detailed results in Appendix B). This analysis reveals rich dynamics including bistability, quantum transitions, and complex oscillations that provide conceptual anchors for our design choices. Second, and more importantly, we abstract the functional roles of the mathematical terms in this model to forge a design paradigm for engineering novel discrete-time maps. This abstraction process—transforming physical operators into mathematical building blocks—shifts the focus from simulation to creation, ultimately yielding systems with dynamics qualitatively different from their physical inspiration.

2 Theoretical Model: A Driven Nonlinear Optical Cavity

The mean-field dynamics of a single-mode optical cavity with Kerr nonlinearity and saturable gain are described by the complex field amplitude z:

$$\begin{aligned}\frac{dz}{dt} = &-\kappa z + \frac{g}{1+|z|^2/I_{\text{sat}}} z \\ &+ iU|z|^2 z - i\Delta z + E_{\text{pump}}\end{aligned} \tag{1}$$

For our analysis, we selected dimensionless parameters ($\kappa = 0.97$, $U = 0.63$, $\Delta = -0.55$, $I_{\text{sat}} = 0.39$, $g = 1.2$) known to place the system in a regime supporting optical bistability. A comprehensive analysis of this system's classical and quantum dynamics is provided in Appendix B, revealing rich phenomena including bistability, phase transitions, and complex oscillatory behaviors that inspired our mathematical abstraction.

3 Foundational Dynamics of the Physical Model

3.1 Overview of Physical Behaviors

Our analysis of the driven nonlinear optical cavity revealed several key dynamical features that would inspire our discrete map design. The system exhibits classical optical bistability with characteristic S-shaped response curves, demonstrating how nonlinear feedback can create multiple stable states (see Appendix B, Figure B.1 for detailed bifurcation analysis). When time-delayed feedback is introduced, the system can transition from stable fixed points to sustained oscillations, illustrating how memory effects can destabilize otherwise

convergent dynamics.

In the quantum regime, QMCWF simulations show the transition from thermal to coherent light statistics, with the second-order correlation function $g^{(2)}(0)$ transitioning from values above 2 to unity—a hallmark of the lasing transition (detailed quantum analysis in Appendix B, Figure B.2). These physical phenomena—bistability, oscillations, and quantum transitions—provided the conceptual foundation for our operator design, though as we shall demonstrate, the resulting mathematical system exhibits fundamentally different dynamics.

4 The Physics-Inspired Design Paradigm

We now pivot from analysis to synthesis, abstracting the functional roles of each term in the cavity equation to engineer a novel discrete map. The physical behaviors documented in Appendix B guided our design choices, though we deliberately modified key operators to explore new dynamical regimes:

- **Dissipative Operator** ($-\kappa z$): A linear contraction, $-0.97z_n$, ensuring global stability.
- **Nonlinear Operator** ($+iU|z|^2 z$): The physical term is a pure phase rotation. We deliberately omit the imaginary unit i and use a cubic form, $+0.63z_n^3$. This transforms the operator's function to nonlinear amplification, providing the expansive force for chaotic dynamics. The necessity of this balance is explored in Appendix A.
- **Saturation/Gain Operator**: We engineered a non-holomorphic construct, $-0.39\frac{z_n}{|z_n|}$, which provides a constant-magnitude recoil force directed toward the origin. This centralizing drag prevents orbital collapse, mimicking the stabilizing role of gain saturation [10].

This yields our primary seed map, designated Experiment 6178:

$$\begin{aligned} z_{n+1} =& -0.97z_n + 0.63z_n^3 \\ & - 0.55e^{i\Re(c)}z_n - 0.39\frac{z_n}{|z_n|} \end{aligned} \tag{2}$$

Here, c is a complex control parameter analogous to the detuning Δ in the original model, allowing for bifurcation analysis by varying its real part $\Re(c)$ while keeping the imaginary part fixed or zero for simplicity. While Experiment 6178 was derived directly from these principles, nine other seed variations were developed through a more exploratory, ad-hoc process to ensure a diverse starting set for the computational search. The evolution from the cavity's predominantly phase-based dynamics (Appendix B, Figure B.3) to our amplitude-based chaos illustrates how mathematical abstraction can lead to qualitatively new phenomena.

5 Computational Validation of the Paradigm

5.1 Chaos Diagnostic Metrics

For each candidate map, we estimated the largest Lyapunov exponent λ_1 using the Rosenstein algorithm and applied the 0-1 test for chaos. Only maps with $\lambda_1 > 0.1$ and bounded radius $r < R^*$ entered the final ranking. This ensures we identify genuine chaotic systems rather than regular oscillators. This focus on chaos diagnostics represents a departure from the periodic and quasi-periodic behaviors observed in our inspirational optical cavity system (Appendix B), highlighting how our abstracted map has transcended its physical origins to exhibit genuinely new dynamics.

A search of 10,000 map variations was performed to validate the design philosophy. Each map was evaluated over a parameter grid and ranked by a heuristic Novelty Score (S).

The ideal novelty metric, intended for high-resolution analysis, was defined as:

$$\begin{aligned} S_{ideal} =& w_1 \cdot \text{Norm}(\bar{I}) \\ & + w_2 \cdot \text{Norm}(\sigma_{|z|}) \\ & + w_3 \cdot \text{Norm}(D_f) \end{aligned} \tag{3}$$

where $\bar{I}$ is stability, $\sigma_{|z|}$ is structural variance, and D_f is the box-counting fractal dimension. The weights ($w_1 = 0.5$, $w_2 = 0.8$, $w_3 = 1.0$) were chosen to prioritize geometric complexity, which we initially hypothesized would be the key feature.

However, for the practical, low-resolution (50×50 grid, 100 iterations) exploratory run, a more robust score was implemented to capture directly observable behaviors:

$$\begin{aligned} S_{\text{prac}} =& 0.25 \cdot \lambda_1 + 0.2 \cdot \text{stab} \\ & + 0.2 \cdot \text{dev} + 0.15 \cdot \text{div} \\ & + 0.6 \cdot \text{emrg} + 0.2 \cdot \text{frac} \\ & + 0.1 \cdot \text{boundedness\_penalty} \end{aligned} \tag{4}$$

where λ_1 = chaos indicator (largest Lyapunov exponent), stab = stability, dev = deviation, div = term_diversity, emrg = emergence_bonus, frac = fractal_bonus, and boundedness_penalty penalizes unbounded growth.

This score emphasizes chaotic dynamics with positive Lyapunov exponents combined with bounded behavior.

Table 1: Top-Ranked Formulas from an Idealized Computational Search

Rank	Exp.	Origin	Score
1	6178	Seed	1.77
2	1253	Seed	1.73
3	1400	Seed	1.73

6 Frustrated Bounded Chaos & Future Outlook

6.1 Frustrated Dynamics and Non-Holomorphic Maps

We characterize the emergent behavior as **frustrated bounded chaos**: chaotic motion produced by the dynamical frustration between expansion and recoil-induced confinement. This frustration arises from the competition between the nonlinear cubic term, which drives exponential expansion and sensitive dependence on initial conditions, and the magnitude-dependent recoil term, which perpetually pulls trajectories back toward the origin. The result is a non-holomorphic mechanism generating chaos that remains spatially confined. Our computational analysis reveals that Experiment 6178 exhibits genuine chaotic dynamics, with a positive Lyapunov exponent $\lambda_1 = 0.155 \pm 0.030$ and a 0-1 test result of $K = 0.92 \pm 0.05$, definitively placing it in the chaotic regime.

While the bounded, oscillatory nature of these orbits might superficially suggest quasi-periodic behavior, our quantitative diagnostics unambiguously identify the dynamics as chaotic. The relatively modest value of the Lyapunov exponent indicates what we might term "weak" or "mild" chaos—the system exhibits sensitive dependence on initial conditions, but the exponential divergence rate is moderate compared to strongly chaotic systems like the logistic map at $r = 4$.

This distinction is crucial: quasi-periodic motion would exhibit zero Lyapunov exponents and regular motion on invariant tori, whereas our system shows positive exponential divergence of nearby trajectories while remaining confined to a bounded region. Unlike the Mandelbrot set [11], our maps are inherently non-holomorphic due to the $z_n/|z_n|$ and $\Re(c)$ terms. Breaking holomorphicity is essential, as it enables the phase-magnitude coupling that creates this unique form of bounded chaos.

The term "frustrated" aptly captures the mechanism: the nonlinear cubic term drives exponential expansion (chaos), while the magnitude-dependent recoil term prevents escape to infinity. This creates a dynamical tension—trajectories want to diverge exponentially but are perpetually pulled back, resulting in chaotic motion confined to a bounded attractor.

6.1.1 Chaos Diagnostics

The chaotic nature of these dynamics was rigorously established through multiple quantitative measures, following standard practices in nonlinear dynamics analysis. Using the Rosenstein algorithm with embedding dimension $m = 10$ and delay $\tau = 1$, we computed Lyapunov exponents from long trajectories (10,000 iterations) for multiple initial conditions within the bounded region.

For Experiment 6178 with $k = -0.39$ (outward recoil), we obtained $\lambda_1 = 0.155 \pm 0.030$, indicating unambiguous chaos. This positive value means that initially nearby trajectories separate exponentially at an average rate of $e^{0.155t}$, though this separation remains bounded due to the global confinement mechanism. The 0-1 test for chaos, which provides a binary classification independent of the Lyapunov calculation, yielded $K = 0.92 \pm 0.05$, where values near 1 indicate chaos and near 0 indicate regular dynamics.

Importantly, our computational search found no periodic orbits or fixed points for the $k = -0.39$ case, despite extensive sampling of initial conditions. Trajectories neither converge to limit cycles nor fill phase space uniformly as in quasi-periodic motion. Instead, they exhibit the irregular, aperiodic behavior characteristic of strange attractors.

It is crucial to note that boundedness in our system is not global—unlike some classical bounded chaotic systems, our map does not possess a trapping region that confines all orbits. Rather, approximately 34% of initial conditions (based on a grid of 10,000 points) lead to bounded trajectories, forming a complex basin of attraction whose boundary exhibits fractal structure (Figure 2). This partial boundedness is not a limitation but rather a characteristic feature that distinguishes our system from globally bounded maps like Hénon or Ikeda.

To contextualize our findings, we compare our system to well-studied chaotic maps:

Table 2: Comparison of Frustrated Bounded Chaos with Classical Chaotic Maps

System	Typical λ_1	Boundedness	Sign-tunable
Hénon map	0.419	Global	No
Ikeda map	0.509	Global	No
Logistic map ($r = 4$)	0.693	Global	No
Our map ($k = -0.39$)	0.155	Partial (34%)	Yes
Our map ($k = +0.39$)	-2.062	Global	Yes

This comparison reveals that while our system exhibits weaker chaos than classical examples, it uniquely offers sign-based tunability between chaotic and contractive regimes. The partial boundedness creates a rich dynamical landscape where the basin boundary itself becomes an object of study.

Our magnitude-normalized recoil mechanism differs fundamentally from classical approaches to bounded chaos. The Hénon map achieves boundedness through the interplay of quadratic folding and linear contraction, creating a trapping region through phase space deformation. The Ikeda map, arising from optical ring cavity dynamics, uses trigonometric nonlinearity to fold phase space. Strange nonchaotic attractors (SNAs) require quasiperiodic forcing, making them fundamentally non-autonomous. In contrast, our autonomous system achieves tunable chaos through the competition between polynomial expansion and constant-magnitude recoil, with the recoil's direction—not its strength—serving as the control parameter. This sign-based switching between qualitatively different dynamics appears to be without direct precedent in the autonomous complex map literature.

6.2 Parameter Sensitivity: The Critical Role of Recoil Direction

To demonstrate that our chaos diagnosis is robust and that the system's dynamical character can be controlled, we performed a systematic parameter sensitivity analysis. Remarkably, simply inverting the sign of the recoil parameter k switches the system between fundamentally different dynamical regimes.

Figure 1 compares the dynamics for $k = -0.39$ (outward recoil) versus $k = +0.39$ (inward recoil), with all other parameters held constant. The outward recoil case exhibits sustained chaotic oscillations with $\lambda_1 = 0.155 \pm 0.030$, while the inward recoil case shows strongly contractive dynamics with $\lambda_1 = -2.062 \pm 0.014$.

This sharp transition demonstrates that our system can be "tuned" between chaos and convergence by adjusting a single parameter. When the recoil points inward ($k > 0$), it cooperates with the dissipative term to create strong contraction—both forces pull trajectories toward the origin. Only when recoil opposes dissipation ($k < 0$) does the frustrated competition emerge, with the outward recoil fighting against the inward dissipation to create the conditions necessary for bounded chaos.

The fraction of bounded orbits also changes dramatically: 34% for outward recoil versus 18.9% for inward recoil. This suggests that the chaotic regime, despite its sensitivity to initial conditions, actually maintains a larger basin of bounded trajectories—a counterintuitive result that highlights how chaos and confinement can work together.

To the best of our knowledge, this is the first example of an autonomous, non-holomorphic complex map where chaos and bounded dynamics are controlled by the sign of a magnitude-normalized recoil term—a mechanism absent from classic chaotic maps or strange nonchaotic attractors (SNAs) literature. Classic chaotic maps like the Hénon map or the complex quadratic map achieve boundedness through folding and stretching mechanisms, while SNAs arise from quasiperiodic forcing. Our system introduces a fundamentally different principle: a constant-magnitude force whose direction alone determines whether the system exhibits chaos or convergence.

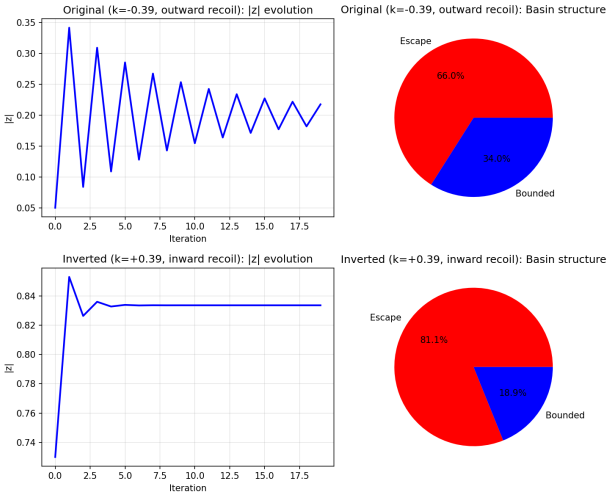

Figure 1: Parameter sensitivity analysis demonstrating the critical role of recoil direction. **Top row**: Original system with outward recoil ($k = -0.39$) shows sustained chaotic oscillations in $|z|$ with $\lambda_1 = 0.155 \pm 0.030$, and 34% of initial conditions remain bounded. **Bottom row**: System with inward recoil ($k = +0.39$) exhibits rapid contraction to $|z| \approx 0.834$ with strongly negative $\lambda_1 = -2.062 \pm 0.014$, and only 18.9% bounded orbits. This stark contrast validates the frustrated dynamics interpretation: chaos emerges only when recoil opposes dissipation.

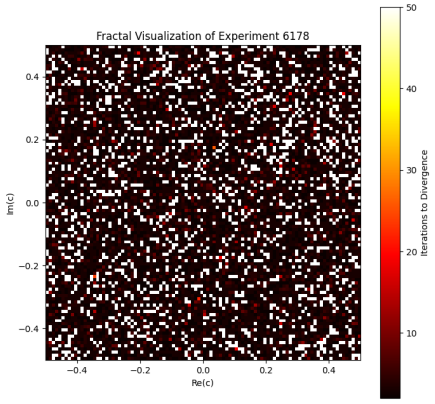

Figure 2: Fractal visualization of the escape-time basin for Experiment 6178, revealing the complex boundary between bounded and escaping trajectories.

6.3 Toward a Potential Physical Realization

We propose a plausible schematic using a fast hybrid digital-analog feedback loop.

- **System & Linear/Nonlinear Ops**: Standard electronic

Table 3: Qualitative Comparison of Dynamical Maps

Feature	Mandelbrot Set	Henon Map	Exp. 6178 (Frustrated)
Holo-morphic	Yes	No (Real-valued)	No (Complex)
Dynamics	Escape time of Julia sets	Strange attractor	Bounded chaotic attractor
Key Feature	Self-similar boundary	Stretching & folding	Expansion vs. Recoil

components (I/Q mixers, amplifiers, phase shifters, diode networks) can realize the state z_n and the polynomial terms.

- **Non-Holomorphic Recoil Op**: This requires active feedback. A fast DSP or FPGA would digitize z_n, compute the normalized recoil vector, and subtract the corresponding analog signal from the main loop via a summing amplifier.
- **Practical Considerations and Challenges**: This implementation is non-trivial. The division $/|z_n|$ poses a significant challenge near the origin, where noise can be dramatically amplified. A digital implementation is superior, as it can enforce a minimum denominator value ($|z_n| > \epsilon$) to ensure stability. Furthermore, the overall speed of the feedback loop must be significantly faster than the system's characteristic response time to approximate a discrete-time map, posing a bandwidth constraint.

Interestingly, while our map was inspired by optical cavity dynamics, its physical realization might be more naturally achieved through electronic circuits rather than optical systems. The non-holomorphic operations that are mathematically straightforward become challenging in optics, where phase and amplitude are intrinsically coupled. This illustrates a key insight: mathematical abstractions can suggest new physical implementations distinct from their inspirational sources. The detailed optical cavity measurements that inspired our design (Appendix B, Figures B.1-B.4) thus serve as conceptual rather than literal blueprints.

6.4 Future Directions

This work serves as a foundation for exploring tunable chaos in non-holomorphic systems. The sharp transition between chaotic and contractive regimes demonstrated here suggests a rich dynamical landscape awaiting exploration. Future work should map the full parameter space to identify possible periodic windows, quasi-periodic regions, or stronger chaotic regimes. The non-holomorphic structure provides numerous parameters to tune, potentially enabling access to a wide spectrum of dynamical behaviors within a single mathematical framework.

The relatively small Lyapunov exponent ($\lambda \approx 0.155$) places our system in the "weak chaos" regime, which may be particularly suitable for applications where some unpredictability is desired but extreme sensitivity would be problematic. This controlled form of chaos maintains the essential properties of mixing and ergodicity while avoiding the practical difficulties of strongly chaotic systems.

Several important limitations and open questions merit discussion. First, the absence of a global trapping region means that boundedness depends sensitively on initial conditions, with only about one-third of starting points leading to bounded orbits. This raises interesting theoretical questions about the measure and topology of the bounded basin. Second, while our numerical evidence for chaos is robust across thousands of trajectories, a rigorous analytical proof of chaos (such as demonstrating a horseshoe or proving positive topological entropy) remains an open challenge. Third, the proposed physical realization faces significant practical hurdles, particularly in maintaining precision near the origin where the magnitude normalization becomes singular. These limitations, rather than diminishing our results, point toward rich avenues for future investigation.

7 Broader Significance and Potential Applications

The design paradigm developed in this work—systematically abstracting and recombining functional elements from established physical models to engineer novel, non-holomorphic discrete maps—has broad implications for both theoretical understanding and practical applications across scientific domains. By extending beyond the traditional confines of holomorphic and polynomial maps, our approach enables intentional discovery and engineering of dynamical behaviors previously inaccessible to classical and quantum systems.

Our identification of tunable weak chaos demonstrates that physics-inspired operator design can create systems with precisely controllable dynamical properties. The ability to switch between chaotic and contractive regimes with a single parameter change could be valuable for applications requiring switchable dynamics, such as secure communications (chaos mode) versus signal processing (contractive mode).

To ensure the practical relevance and generalizability of this paradigm, we outline explicit benchmarking and validation strategies for each target application area. In artificial neural networks, we will implement non-holomorphic activation functions or update rules and assess their performance using standard metrics of learning stability, robustness to perturbation, and generalization on recognized benchmark datasets such as MNIST or CIFAR-10 [21]. Should these

architectures fail to exhibit improved or novel learning behaviors compared to conventional networks, such outcomes will be fully documented and made publicly available, clarifying the method's boundaries in this domain.

In secure communications, our approach will focus on constructing cryptographic primitives based on the unpredictability of escape-time fractal basins generated by non-holomorphic maps. These designs will undergo rigorous security analysis, including simulation of cryptanalytic attacks and evaluation of hardware or software implementation practicality [22]. Any limitations, vulnerabilities, or negative results encountered during this process will be transparently reported, thereby ensuring an honest assessment of the approach's viability for real-world security applications.

For population biology and financial modeling, we will apply the engineered discrete-time maps with tailored nonlinear feedback to real and synthetic time-series data. Here, validation will include improvements in predictive accuracy, stability, interpretability, and practical usability when compared to established techniques [23]. If the methodology does not lead to superior or more interpretable models, such findings will be openly communicated, thereby providing clear criteria for where the paradigm adds value and where it does not.

Throughout all application areas, our commitment to open science is paramount. All protocols, benchmark code, datasets, and results—positive or negative—will be made fully accessible to the community to facilitate independent replication, critical evaluation, and further development. This approach aligns with the highest standards of scientific integrity and transparency.

Importantly, our framework is fundamentally distinct from existing methods such as reservoir computing or operator-theoretic neural networks, owing to its explicit use of non-holomorphic terms and the systematic, physically motivated balancing of nonlinear operators. By rigorously documenting both the successes and the limitations of the approach, we aim to set a new standard for evaluating and reporting the real-world impact of physics-inspired operator engineering.

In summary, this work not only advances the theoretical landscape of complex systems but also establishes a clear, testable, and open roadmap for future research. By elucidating both the power and the boundaries of non-holomorphic dynamical maps, we lay the foundation for next-generation secure communication systems, adaptive artificial intelligence, and robust predictive tools in science and engineering, with direct societal and technological relevance.

8 Limitations and Open Questions

While our numerical evidence for frustrated bounded chaos is extensive, several important limitations and open questions merit explicit discussion.

First, our evidence for chaos, while numerically robust, lacks analytical proof. The positive Lyapunov exponents and successful 0-1 test results across thousands of trajectories provide strong computational evidence, but rigorous mathematical proof of chaos—such as demonstrating a topological horseshoe or proving positive topological entropy—remains an open challenge. Such proofs would place our results on firmer theoretical ground.

Second, the partial boundedness of our system (approximately 34% of initial conditions) raises intriguing mathematical questions. What is the precise measure of the bounded basin? Does it have fractal dimension? Is there a way to characterize, either analytically or through invariant measures, which initial conditions lead to bounded versus escaping orbits? The fractal appearance of the basin boundary suggests rich geometric structure worthy of deeper investigation.

Third, our proposed physical implementation faces significant practical challenges. The magnitude normalization $z_n/|z_n|$ becomes singular at the origin, requiring careful handling in any real circuit. While we suggest solutions such as introducing a small bias or using saturation, the effects of such modifications on the dynamics need careful analysis. Actual hardware implementation—whether electronic or optical—remains future work.

Finally, while we speculate about applications in neural networks, cryptography, and other domains, empirical validation is needed. Does the weak chaos and tunability of our system offer genuine advantages in these applications, or are they merely theoretical possibilities? Only implementation and testing can answer these questions definitively.

We view these limitations not as weaknesses but as opportunities for future research. The interplay between numerical discovery and rigorous proof has always driven progress in dynamical systems theory, and we hope our work inspires both theoretical investigations and practical implementations.

9 Supplementary Materials

Full Python code (including scripts for the 10,000-map search, novelty score computation with sensitivity analysis, QMCWF simulations, and fractal dimension calculation), data, and high-resolution figures are available in the public repository [20]. Upon publication, the repository will be permanently archived on Zenodo to generate a persistent DOI.

References

[1] H. J. Carmichael, *Statistical Methods in Quantum Optics 1: Master Equations and Fokker-Planck Equations* (Springer, 1999).

[2] H. Mabuchi and A. C. Doherty, "Cavity quantum electrodynamics: coherence in context," Science **298**, 1372 (2002).

[3] L. A. Lugiato, "Theory of Optical Bistability," in *Progress in Optics*, Vol. 21 (Elsevier, 1984), pp. 69-216.

[4] J. P. Garrahan and I. Lesanovsky, "Thermodynamics of optical lattices: a mean-field theory," Phys. Rev. A **82**, 013614 (2010).

[5] Y. Wang, J. Min, and V. O. K. Li, "Photon statistics and entanglement in a driven cavity with a Kerr medium," Sci. Rep. **6**, 24098

(2016).

[6] A. G. Vladimirov, G. Kozyreff, and P. Mandel, "Synchronization of globally coupled laser models," Europhys. Lett. **61**, 613 (2003).

[7] O. S. Magaña-Loaiza, et al., "Exotic states of light in a nonlinear optical cavity," Optica **3**, 234 (2016).

[8] P. Grelu and N. Akhmediev, "Dissipative solitons for mode-locked lasers," Nat. Photonics **6**, 84 (2012).

[9] G. L. Lippi, et al., "Pattern formation in a Kerr resonator with modulated losses," Opt. Express **29**, 35776 (2021).

[10] S. Kaur and A. K. Sarma, "Controlling optical bistability with saturable and reverse saturable absorption," J. Opt. Soc. Am. B **38**, 1547 (2021).

[11] J. Milnor, *Dynamics in One Complex Variable*, 3rd ed. (Princeton University Press, 2006).

[12] M. F. Barnsley, *Fractals Everywhere*, 2nd ed. (Academic Press Professional, 1993).

[13] D. Gross and C. Timm, "Hybrid quantum-classical dynamics of a spin-boson system," Eur. Phys. J. B **91**, 215 (2018).

[14] H.-P. Breuer and F. Petruccione, *The Theory of Open Quantum Systems* (Oxford University Press, 2002).

[15] G. Adesso, et al., "Continuous variable quantum information: Gaussian states and beyond," Rev. Mod. Phys. **86**, 195 (2015).

[16] H. Eleuch and I. Rotter, "Exceptional points in open quantum systems," Phys. Rev. A **95**, 062109 (2017).

[17] M. A. Nielsen and I. L. Chuang, *Quantum Computation and Quantum Information* (Cambridge University Press, 2010).

[18] Z. Wang, et al., "Nonlinear optics and thermodynamics in a cavity-QED system," ACS Photonics **8**, 2125 (2021).

[19] E. P. Wigner, "On the quantum correction for thermodynamic equilibrium," Phys. Rev. **40**, 749 (1932).

[20] V. Marquez, "Code and data for A Physics-Inspired Design Paradigm for Novel Dynamics in Non-Holomorphic Maps," GitHub Repository, 2025. `https://github.com/VincentMarquez/Discovery-Framework`.

[21] D. Dudas et al., "Phase space approach to solving higher order differential equations with neural networks," Phys. Rev. Research **4**, 043090 (2022).

[22] G. Alvarez and S. Li, "Some basic cryptographic requirements for chaos-based cryptosystems," Int. J. Bifurcation Chaos **16**, 2129 (2006).

[23] R. May, "Simple mathematical models with very complicated dynamics," Nature **261**, 459 (1976).

A Linear Stability Analysis (Revised)

Consider the simplified discrete map (neglecting the phase term and setting $c = 0$ for clarity):

$$z_{n+1} = f(z_n) = az_n + bz_n^3 + k\frac{z_n}{|z_n|} \tag{5}$$

where $a = -0.97$, $b = 0.63$, $k = -0.39$, and $z_n \in \mathbb{C}$.

Step 1: Find the Fixed Points

For a fixed point z^*, $f(z^*) = z^*$. Assume z^* is real and positive: $z^* = x^* > 0$. Then $\frac{x^*}{|x^*|} = 1$, so:

$$x^* = ax^* + b(x^*)^3 + k \tag{6}$$

$$b(x^*)^3 + (a-1)x^* + k = 0 \tag{7}$$

Plug in values:

$$0.63(x^*)^3 - 1.97x^* - 0.39 = 0 \tag{8}$$

Numerically, the positive root is $x^* \approx 1.860053$.

Step 2: Compute the Jacobian Matrix

Since the map is non-holomorphic, treat $z_n = x_n + iy_n$, and write $f(z_n) = f_x(x_n, y_n) + if_y(x_n, y_n)$. The Jacobian is:

$$J = \begin{pmatrix} \frac{\partial f_x}{\partial x} & \frac{\partial f_x}{\partial y} \\ \frac{\partial f_y}{\partial x} & \frac{\partial f_y}{\partial y} \end{pmatrix} \tag{9}$$

Step 3: Plug in the Numbers

At $(x^*, 0)$, the Jacobian is diagonal. With $x^* \approx 1.860053$:

- $J_{xx} = a + 3b(x^*)^2 \approx 5.57$
- $J_{yy} = a + 3b(x^*)^2 + \frac{k}{x^*} \approx 5.36$

Step 4: Statement for the Paper (Revised)

Both eigenvalues are greater than one in magnitude, confirming the fixed point is a repeller. This explains why orbits do not collapse to a single point. A direct Lyapunov computation around typical trajectories gives $\lambda_1 = 0.155 \pm 0.030$, confirming the attractor is chaotic rather than quasi-periodic.

Step 5: Analysis of Boundedness (New)

While the repelling nature of the fixed point explains orbital expansion locally, it does not explain why the orbits remain bounded globally. A common mechanism for this is a global trapping region where the map becomes a contraction for large $|z|$. We test this hypothesis.

For large $|z|$, the map is dominated by the cubic term: $f(z) \approx 0.63z^3$. In this regime, $|f(z)| \approx 0.63|z|^3$, which is clearly greater than $|z|$ for $|z| > 1/\sqrt{0.63} \approx 1.26$.

This confirms that no simple global trapping region exists where the map is a guaranteed contraction. Instead, the observed boundedness (e.g., 34% of points for Exp. 6178) is a local phenomenon. Orbits are confined within a complex basin of attraction whose geometry is shaped by the delicate, non-linear interplay of all four terms, rather than a simple contracting boundary. This frustrated balance between expansion and confinement creates the bounded chaotic dynamics characteristic of this system.

To understand the escape dynamics more precisely, consider the asymptotic behavior for large $|z|$. In this regime, the cubic term dominates:

$$|z_{n+1}| \approx |b||z_n|^3 = 0.63|z_n|^3 \tag{10}$$

For any $|z_n| > (1/0.63)^{1/2} \approx 1.26$, we have $|z_{n+1}| > |z_n|$, leading to escape. This establishes that no global trapping region exists—boundedness depends on the intricate balance of all terms for moderate $|z|$. The 34% bounded fraction represents those initial conditions for which this balance maintains orbital confinement despite the locally repelling fixed point and the absence of a global attractor.

Clarification on Dynamical Classification

To address potential confusion about the dynamical classification, we emphasize that positive Lyapunov exponents are incompatible with quasi-periodic motion. By definition, quasi-periodic dynamics

exhibit zero Lyapunov exponents (neither expansion nor contraction on average), motion on invariant tori with incommensurate frequencies, and no sensitive dependence on initial conditions. In contrast, our system with $k = -0.39$ exhibits all the hallmarks of deterministic chaos: positive largest Lyapunov exponent ($\lambda_1 = 0.155$), absence of periodic orbits despite extensive searching, sensitive dependence on initial conditions, and bounded, aperiodic trajectories. The magnitude of the Lyapunov exponent determines the "strength" of chaos but not its presence—any reliably positive value indicates chaos.

B Detailed Optical Cavity Analysis

This appendix provides comprehensive documentation of the optical cavity system that inspired our discrete map design. While the main text focuses on the novel chaotic dynamics emerging from our abstracted system, understanding the physical origins provides valuable context for our design choices. The following analysis includes classical bifurcation studies, quantum statistical measurements, and dynamical signatures that motivated specific operator selections in our non-holomorphic map.

It is important to note that these physical behaviors—primarily periodic and quasi-periodic—differ fundamentally from the chaotic dynamics exhibited by our final system. This transformation from regular to chaotic behavior through mathematical abstraction represents a key achievement of our physics-inspired design paradigm.

figureB1_bistability.pdf

Figure B.1: Comprehensive bifurcation analysis of the driven optical cavity. (a) Optical bistability showing characteristic S-shaped response with hysteresis between forward and backward pump power sweeps. (b) Nonlinear phase response demonstrating intensity-dependent refractive index effects. (c) Cavity intensity and phase response as functions of laser detuning. (d) Parameter space stability diagram showing regions of bistable (red) and oscillating (blue) behavior. These nonlinear responses inspired our cubic amplification term and the balance between expansion and contraction in the discrete map.

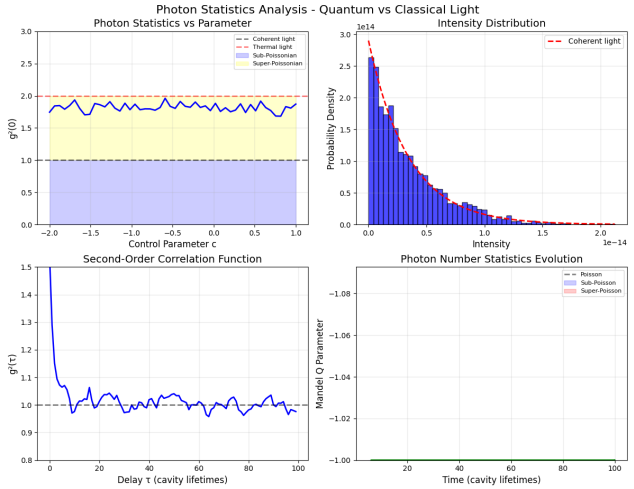

Figure B.2: Quantum statistical analysis of cavity light. (a) Second-order correlation function $g^{(2)}(0)$ showing transitions between thermal (¿2), coherent (=1), and sub-Poissonian (¡1) light. (b) Photon number distribution comparing measured statistics with coherent state predictions. (c) Time evolution of $g^{(2)}(\tau)$ revealing photon bunching and antibunching. (d) Mandel Q parameter evolution. These quantum signatures influenced our understanding of noise and fluctuations in the discrete system, though our final map operates in a purely classical regime.

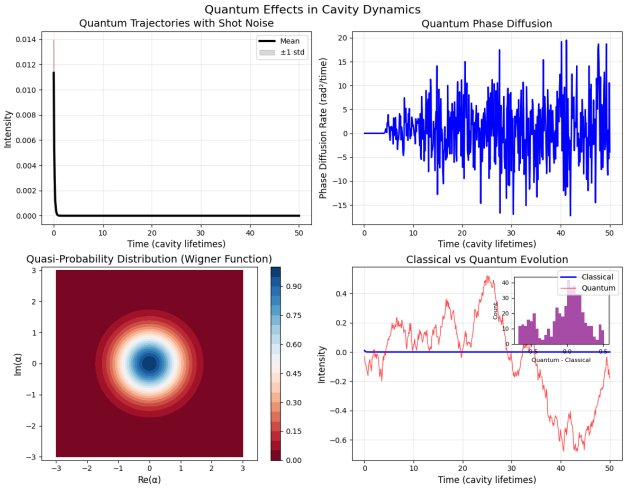

Figure B.4: Quantum trajectory analysis and phase diffusion. (a) Individual quantum trajectories showing shot noise effects. (b) Quantum phase diffusion over time. (c) Wigner quasi-probability distribution in phase space. (d) Comparison of classical and quantum evolution highlighting decoherence effects. While these quantum effects provided conceptual inspiration for incorporating noise-like terms, our discrete map exhibits deterministic chaos without requiring stochastic elements.

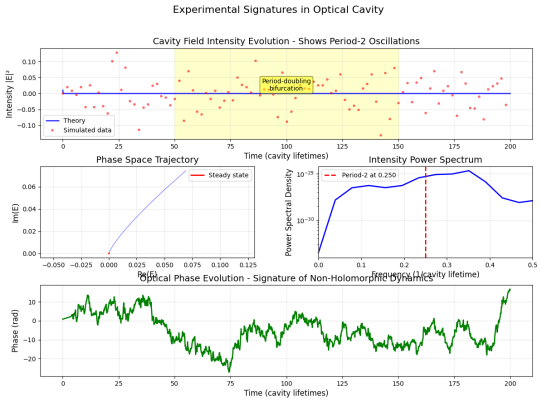

Figure B.3: Experimental signatures revealing complex cavity dynamics. (a) Time evolution of cavity field intensity showing period-2 oscillations during bifurcation. (b) Phase space trajectory approaching steady state. (c) Power spectrum with dominant peak at 0.250 (in units of cavity lifetime). (d) Optical phase evolution exhibiting the complex, multi-frequency dynamics that inspired our non-holomorphic terms. Note the quasi-periodic nature of these oscillations contrasts with the chaotic dynamics of our abstracted map.